Numerical modelling of a latent heat storage system in a stovepipe

Alexis Sevault[a]*, Jerol Soibam[b], Nils Erland L. Haugen[a,b], Øyvind Skreiberg[a]

[a] SINTEF Energy Research, P.O.Box 4761 Torgarden, NO-7465 Trondheim, Norway

[b] NTNU - Norwegian University of Science and Technology, Dpt of Energy and Process Engineering, 7491 Trondheim, Norway

* Corresponding author. Tel.: +47 4101 9994 - E-mail address: Alexis.Sevault@sintef.no

Abstract

Latent heat storage (LHS) is a promising concept for small-scale batch combustion. E.g. wood log stoves rely on a batch combustion process, yielding a transient heat production with high peak effect. A well-designed LHS system with phase change materials (PCM), with melting temperature in the range of 100-150 °C, can flatten out the peak heat release and instead release the heat to the room over an extended time-period. The objective of the current study was to design a compact and durable LHS system capable of storing a substantial part of the heat release during the combustion phase and to effectively release the stored heat to the room for 6 to 10 hours after the combustion phase ends. A passive LHS system designed as a coaxial cylinder acting as a stovepipe located at the top of a wood stove was simulated by utilizing a transient two-dimensional axisymmetric approach with the CFD tool ANSYS FLUENT. The heat exchanger was equipped with internal metallic fins to enhance the conductivity and even out the temperature distribution inside the PCM.

Various fin configurations were evaluated and it was found that configurations with three equidistant radial fins along the 300-mm long inner pipe provided the best heat distribution in the PCM. The effect of fin lengths was investigated through a parametric study using four different fin lengths within the PCM domain. Using 17.5-mm or 52.5-mm fins in the 70-mm PCM layer yielded the best trade-off for the application. This configuration enabled achieving a slow but close to complete melting of the PCM within a realistic combustion duration, while avoiding overheating the PCM bulk above the degradation temperature. Thereafter, the discharge allowed a slow heat release of the stored latent heat for 6 to 10 hours.

A few recommendations are pointed out, notably the need to study more advanced fin configurations. Another challenge is the thermal degradation of the selected PCM, erythritol, occurring only 42 °C, or less, above its melting temperature. This critical temperature may be reached in the layer close to the hot exhaust gas due to the highly transient combustion behavior of the batch-combustion stoves, endangering the durability of a practical LHS system.

Keywords:

Phase Change Materials, PCM, Thermal Energy Storage, Latent Energy Storage, Wood Stove, Stovepipe

1 Introduction

1.1 Background

Thermal energy storage (TES) is needed whenever there is a temporal mismatch between production and demand of thermal energy. TES can be used to store heat or cold during periods of overproduction of heat or electricity, to be able to utilize it at a later point of time. A classical, and the most obvious, example is solar energy applications (Gil et al., 2010; Hoshi et al., 2005). However, TES may also be applied to reduce peak heating and cooling demands and to improve system efficiency wherever there is a variation in the availability and/or demand, on shorter or longer time scales.

Thermal energy can be stored either in the form of sensible heat, latent heat, or as thermochemical energy (Fleischer, 2015). In a sensible heat storage, heat is stored by heating a medium with high specific heat capacity. In a thermochemical heat storage, heat is stored using reversible chemical reactions that absorb or release thermal energy. In the case of latent heat storage, heat is stored as the latent heat of phase change: melting or vaporization. Latent heat is unique in that the temperature of the material remains around the phase change temperature during the whole phase change process. A great advantage of latent heat storage

is its high energy density as compared to sensible heat storage, resulting in smaller storage volumes. Their high latent heat of fusion enables PCMs to store 5–14 times more heat per unit volume than common sensible storage materials such as water, masonry, or rock (Sharma et al., 2009). Practical phase change materials (PCMs) are materials that undergo solid-liquid transformation, i.e. a melting-solidification cycle, at around the operating temperature range of the selected thermal application (Fleischer, 2015).

Latent heat storage (LHS) for small-scale batch combustion is a promising concept to exploit the properties of PCMs. For example, wood log stoves rely on a batch combustion process, yielding a transient heat production with high peak heat release during combustion, often exceeding the actual needs of the end users. Typical modern wood stoves have a thermal efficiency of 70 to 80 % at nominal load and often produce more heat, especially in highly-insulated buildings, than actually required to heat up the house (Georges et al., 2013). At the end of a batch, the heat release rapidly decreases, while the need for heating may remain.

A well-designed LHS system (with phase change in the range of 100-150 °C) can flatten out the peak heat release to the room by storing it as latent heat, before releasing it to the room again at the end of the combustion cycle. This results in a relatively stable heat release over an extended time-period. PCMs have the potential to yield a more efficient solution than current sensible heat storage solutions using e.g. soapstone. Indeed, PCM can store more heat both per mass and volume and offer a more stable heat release due to the close to isothermal phase change process, while being relatively compact and lightweight. This is of special interest for the highly-insulated low-energy buildings and passive houses. Such LHS systems using PCM may also be designed as a retrofit to existing wood stoves. However, designing an optimal system with a suitable PCM remains challenging due to the complexity of the physical and thermal interactions between PCM, heat source and heat sink.

1.2 Objective

The objective of the current study was to design a compact and durable LHS system capable of storing a substantial part of the heat release during combustion and to effectively release the stored heat to the room at the end of the combustion period, for 6 to 10 hours. A passive LHS system designed as a coaxial cylinder wrapped around a stovepipe located at the top of a wood stove was simulated using transient two-dimensional axisymmetric CFD modelling with ANSYS FLUENT 17.2.

One of the challenges was to exploit a significant part of the heat available in the flue gas, without reducing the draught in the chimney below a critical point, since this could alter the combustion process, which is based on natural draught. Another challenge was to ensure melting of most of the PCM mass within a reasonable time, without overheating part of the PCM, above its degradation temperature. The key findings and detailed results of the parametric study with varying fin length are presented.

1.3 Literature review

With a large variety of available PCMs, and a high number of properties affecting their suitability to a given application. A method was developed to assist the selection process of an optimal PCM for LHTES with wood stove combustion based on a one-dimensional analysis providing key indicators (Kristjansson et al., 2016). The performance of the LHTES is described through the energy density, the ratio of latent to sensible heat capacity, the Biot number and an indicator of overheating risk. These indicators allow effective ranking of PCMs selected for

a given application. For example, a LHTES with the lowest achievable Biot number is preferable for a close to constant heat release of the system during solidification of the PCM.

Regarding similar geometries to the one selected in the present study, Al-Abidi et al. (2013a, 2013b) reported on a successful numerical and experimental study of a LHTES system applied to a liquid desiccant air-conditioning system. The study relied on a triplex tube heat exchanger with internal and external longitudinal fins, where the PCM (with phase change in the range of 77-85 °C) was enclosed between the two concentric tubes. Results showed that the effect of fin thickness was small compared to the fin length and number of fins, which had a strong effect on the time for complete melting and solidification.

With a similar geometry in a lower temperature range, Almsater et al. (2017) presented a CFD model of LHTES in a vertical triplex tube subject to free convection and its validation through experimental results. The heat transfer fluid circulated in the outer and inner tubes, while the central space contained the PCM. Eight longitudinal fins were included to separate the PCM compartments. Water was used as PCM. It was found that the melting phase change duration was generally quicker compared to the freezing process due to free convection.

Various studies investigated the opportunities for thermal energy storage associated to wood stoves. Benesch et al. developed a CFD-based methodology for the analysis and optimization of a wood log stove with sensible heat storage device (Benesch et al., 2015). The results enabled to test different storage materials in solid state. The same group also developed guidelines for heat storage units based on phase change materials, still addressing wood stoves (Mandl & Obernberger, 2017). It was notably pointed out that the PCM melting temperature should not be too high to allow charging at partial combustion load. The following criteria were listed as the most important and challenging: low flammability, low thermal degradation, high heat capacity, high density, suitable melting temperature, affordability, low corrosivity and low toxicity. The advised approach in the guidelines was however the full integration by the side(s) of the stove allowing the flue gas to circulate through the PCM and to discharge heat with the assistance of air channels and free convection.

Another study involving a wood stove manufacturer focused on the technical design and construction of a stove surrounded by plates filled with salt hydrates melting at 60 °C (Zielke et al., 2013). The goal was to avoid firing at the stoves at partial load at night and the high associated emissions, while keeping the house warm. Though the results proved positive, the solution has not yet been commercialized due to the difficulty to achieve a commercial design in line with the customers' expectations.

2   Methodology

2.1.1   Moving boundary problems

Phase change processes exhibit a transient and non-linear behavior with a moving liquid-solid interface and involve flow patterns that are associated with heat transfer in fluids. The heat transfer problem in melting and solidification processes is called the moving boundary problems. It is especially complex since the solid-liquid boundary moves depending on the speed at which the latent heat is absorbed or lost at the boundary. While in theory phase change occurs at one defined temperature, in practice it happens over a temperature range, forming a so-called mushy zone (two-phase zone) between liquid and solid. The most widely used numerical method used to effectively model the phase change is the enthalpy formulation method (Comini et al., 1974).

2.1.2 Enthalpy formulation method

Using the enthalpy formulation method, the enthalpy is considered as a temperature-dependent variable and the flow of the latent heat is expressed in terms of volumetric enthalpy as a function of a temperature of the PCM. The enthalpy formulation is one of the most popular fixed-domain methods for solving a Stefan problem. The major advantage is that the method does not require explicit treatment of the moving boundary. To introduce the formulation, the enthalpy function H is defined as a function of temperature over the fixed domain as given by Voller (1990). This method assumes that enthalpy is a sum of sensible and latent heat:

$$H(T) = h(T) + L_f \beta(T) \tag{1}$$

Where *h(T)* is the sensible enthalpy:

$$h(T) = h_{ref}(T_i) + \int_{T_i}^{T_f} c_p dT \tag{2}$$

and h_{ref} is the reference enthalpy at the initial temperature T_i. β is the liquid fraction during the phase change between solid and liquid states and it can be expressed as:

$$\beta = \begin{cases} 0, & \text{if } T \leq T_s \text{ (Solid)} \\ 1, & \text{if } T \geq T_l \text{ (Liquid)} \\ \dfrac{T - T_s}{T_l - T_s}, & \text{if } T_l \geq T \geq T_s \text{ (Mushy)} \end{cases} \tag{3}$$

An essential feature of the enthalpy method is that the conduction equation is valid for both the solid and liquid phases as well as for the solid-liquid interface and hence, there is no need to track the position of the phase change front (Özişik, 1994). The main advantages of this procedure are:

- The equation is directly applicable for the two phases and the mushy zone.
- The temperature is determined at each point and the thermo-physical properties can be evaluated.
- By only observing the temperature field, the position of the two boundaries can be tracked.

2.1.3 Governing equations used in ANSYS FLUENT

The LHTES system has been modelled using ANSYS FLUENT 17.2. The CFD code is based on the finite volume method and allows for phase change simulations of PCM through the enthalpy porosity method. This means that instead of tracking the liquid-solid front explicitly, the liquid-solid mushy zone (partially solidified region) is treated as a porous zone. The porosity in each cell is set equal to the liquid fraction in that cell, which indicates the fraction of the cell volume that is in liquid form. The liquid fraction is computed at each iteration, based on an enthalpy balance (ANSYS, 2015). The continuity, momentum, and energy equations are given below:

Energy equation:

$$\frac{d(\rho H)}{dt} + \nabla\left(\rho \vec{V} H\right) = \nabla(k \nabla T) \tag{4}$$

Continuity equation:

$$\frac{d\rho}{dt} + \nabla(\rho \vec{V}) = 0 \tag{5}$$

Momentum equation:

$$\frac{\partial(\rho\vec{V})}{\partial t} + \nabla(\rho\vec{V}) = -\nabla P + \mu\nabla^2\vec{V} + \rho\vec{g} + \vec{S} \tag{6}$$

Where V is the fluid velocity, ρ is the density, k is the thermal conductivity, μ is the dynamic viscosity, P is the pressure, g is the gravitational acceleration and S is the momentum source term. The momentum source term S, detailed by Al-Abidi et al. (2013a), is defined as:

$$\vec{S} = \frac{C(1-\beta)^2}{\beta^3+\varepsilon}\vec{V} \tag{6}$$

The source term corresponds to the damping term in Darcy's law, and it is added to the momentum equation due to the phase change effect on convection. The term $\frac{C(1-\beta)^2}{\beta^3+\varepsilon}$ is the porosity function, defined by Brent et al. (1988) to make the momentum equations behave similarly to the Carman-Kozeny equations for flows in porous media. The liquid fraction β is defined in Equation (3). The mushy zone constant, C, reflects the kinetic processes in the mushy zone morphology. It describes how steeply the velocity is reduced to zero when the material solidifies, this constant is varied between 10^4 and 10^7. Higher or lower C values may lead to unphysical oscillations in the results. A small computational constant, $\varepsilon = 0.001$, is used to prevent division by zero.

Since the mushy zone constant is an essential parameter to accurately model the melting processes involving convection, simulations were first carried out with a simplified 2D model and several C values within the above-mentioned range. The smallest value of C (10^4) induced unstable and unphysical results. For $C \geq 10^6$, the influence of buoyancy was fully dampened, leading to a fully conduction-driven melting process. A C value of 10^5 enabled convective effects to play a major role in the melting processes and was also the value of choice in the literature within the same temperature range (Al-Abidi et al., 2013b). Therefore $C = 10^5$ was kept for all simulations.

2.2 Geometry

A coaxial cylindrical heat exchanger seemed the most promising geometry for our purpose of replacing the stovepipe above the wood stove with an amount of PCM located between the two concentric tubes. In this way, the PCM can be loaded by the hot exhaust gas flowing through the vertical inner pipe from bottom to top, the heat is released to the surrounding.

In the stainless-steel coaxial cylinder, the inner tube has an outer diameter of 0.15 m, and the outer tube has an outer diameter of 0.3 m. The wall thickness for both tubes is 5 mm, leaving a 70-mm thick layer of PCM around the inner tube. While a longer coaxial cylinder could be considered in commercial applications, a length of 300 mm was kept for the simulation to represent a more acceptable total weight and to reduce the computing time. Fins in the PCM volume, when present, are radial all around the inner tube and are 3-mm thick and made of stainless steel, see Figure 1.

Though longitudinal fins have proved to enhance the melting rate in similar geometries (Al-Abidi et al., 2013b), radial fins can enable a more homogeneous melting process along the concentric pipe. Another advantage with radial fins was the opportunity to model the LHTES

system using 2D axisymmetry, resulting in shorter computing time than any 3D model with longitudinal fins.
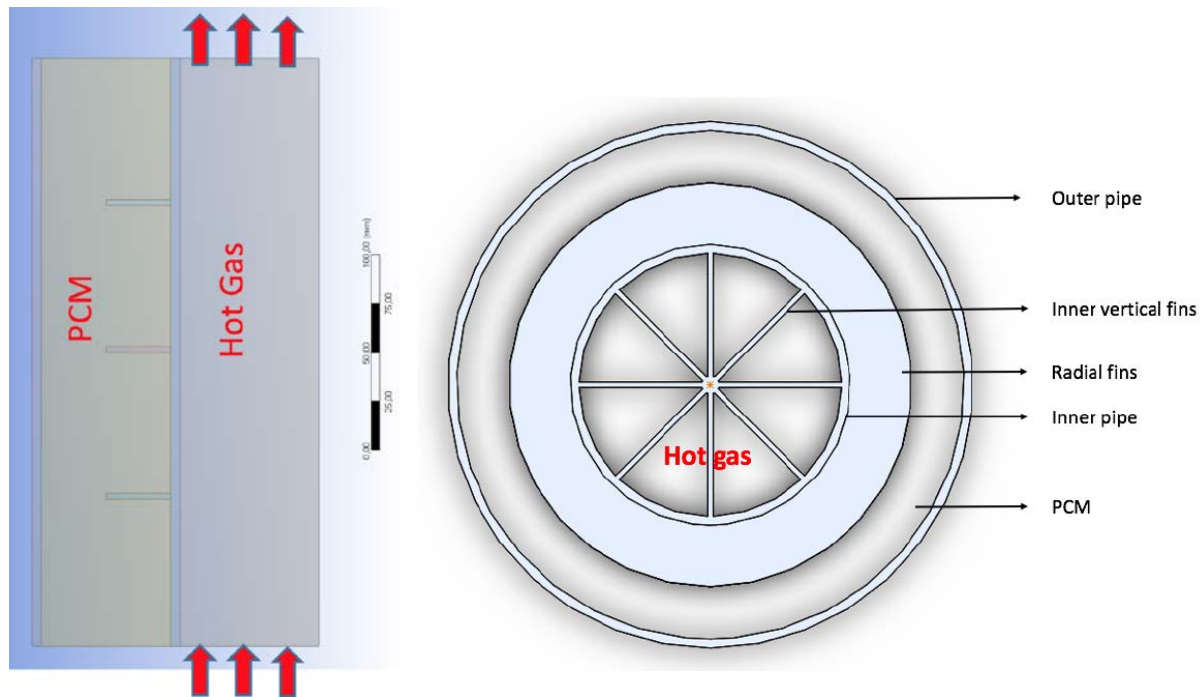
Figure 1: (Left) Coaxial cylinder as modelled in ANSYS FLUENT. Hot exhaust flows through the inner pipe from bottom to top. (Right) Top view of the coaxial cylinder for a radial fin cross section.

A first run of simulations with constant wall temperature and no flowing hot exhaust gas tested the radial fin number and separation distance in the PCM domain, from no fin to three fins equally distributed along the 300-mm long coaxial cylinder. Three equidistant radial fins proved to achieve a more homogenous heat transfer across the PCM and therefore was kept for all simulations (see Figure 1) (Soibam, 2017).

2.3 Material and fluid properties

The hot exhaust gas of batch wood log combustion being in the temperature range 100-250 °C, a PCM such as erythritol was considered due its melting temperature at 118 °C. The thermo-physical properties of erythritol used for the simulations are shown in Table 1. The properties indicated with two temperatures were modelled in ANSYS FLUENT using piece-wise linear equations.

Table 1: Thermo-physical properties of erythritol based on Höhlein et al. (2017), Kaizawa et al. (2008) and Mehling & Cabeza (2008).

Erythritol properties	Values used in simulations
Melting temperature	117-120 °C
Theoretical degradation temperature	160 °C
Latent of heat of solidification	339.9 kJ·kg^{-1}
Specific heat capacity (solid, 20 °C)	1.38 kJ·(kg·K)$^{-1}$
Specific heat capacity (fluid, 140 °C)	2.76 kJ·(kg·K)$^{-1}$
Conductivity (solid, 20 °C)	0.733 W·(m·K)$^{-1}$
Conductivity (fluid, 140 °C)	0.326 W·(m·K)$^{-1}$
Density (solid, 20 °C)	1480 kg·m^{-3}
Density (fluid, 140 °C)	1300 kg·m^{-3}

One challenge with erythritol is its low degradation temperature through decomposition from 160 °C (Kaizawa et al., 2008), while in practice its thermal properties may be altered at even lower temperatures. However, this PCM was kept for the sake of the simulations only due the rest of its thermo-physical properties.

The thermo-physical properties of the hot exhaust gas shown in Table 2 were calculated at 225 °C using GASEQ based on the following composition: 7 % CO_2, 13 % O_2, 20 % H_2O and 60 % N_2. The composition is representative of the exhaust gas flowing out of wood stoves.

Table 2: Exhaust gas properties at 225 °C based on a composition of 7 % CO_2, 13 % O_2, 20 % H_2O and 60 % N_2.

Hot exhaust gas properties	Values used in simulation
Density	0.72 kg·m^{-3}
Specific heat capacity	1155 J·(kg·K)$^{-1}$
Viscosity	2.46.10^{-5} kg·(m·s)$^{-1}$
Conductivity (pure gas)	0.035 W·(m·K)$^{-1}$
Equivalent thermal conductivity with heat transfer enhancement	2.45 W·(m·K)$^{-1}$

The first simulations showed that the heat transfer rate from the hot exhaust gas through the inner tube towards the PCM was insufficient without using any heat transfer enhancement method. Therefore, eight longitudinal fins were considered on the hot exhaust gas side to enhance the heat transfer towards the inner tube (see Figure 1). In the simulations, the fins are represented through the calculated volume-averaged effective heat conductivity of the hot exhaust gas of 2.45 W·(m·K)$^{-1}$ instead of 0.035 W·(m·K)$^{-1}$ for the pure hot gas.

2.4   Computational models in ANSYS FLUENT

The 2D-axisymmetrical geometry was created in ANSYS-workbench DesignModeler as well as the mesh, and then imported to ANSYS FLUENT 17.2. Regarding the model setup, the transient simulations were run with the two-dimensional double-precision code, a pressure-based solver, an absolute velocity formulation, a gravity of 9.81 m·s^{-2}, the energy equation, the *k*-epsilon viscous model and the solidification & melting option.

2.5   Mesh specifications

Due to the solid-liquid phase change, sharp gradients were expected locally. To have a smooth increment in mesh size in the near wall region, the inflation option with smooth transition was used with transition ratio of 0.054 and a growth rate of 1.02 in the PCM domain. A mesh sensitivity analysis yielded an effective resolution of the gradients using a maximum cell size of 1 mm for both the hot gas and the PCM domain, with smaller element size near the walls. The total number of finite elements in the mesh amounted to about 65 000.

2.6   Initial and boundary conditions

For the charging process (melting), the inlet boundary in the gas domain was set to a velocity-inlet with a value of 1 m·s^{-1}, and a constant inlet temperature of 225 °C to simulate the hot exhaust gas flowing through the stovepipe. The outlet boundary in the gas domain was set as an outlet-vent. The outer pipe wall towards the room was set to have mixed thermal conditions, i.e. heat is transferred to the outside due to convection and radiation. The heat transfer coefficient for convection was set to 25 W·m^{-2}·K^{-1} with a free-stream temperature of

298 K. The coefficient was chosen higher than for regular free convection in order to represent the effect of the convective air flows originating from the hot wood stove underneath the stovepipe. For the radiation, the wall emissivity was set to 0.85. The bottom and top walls of the PCM domain were defined as adiabatic walls. The whole LHTES system temperature was set to 298 K as the initial condition.

Given the gas properties and velocity of the hot exhaust, the Reynolds number was within the turbulent regime for a pipe flow, justifying the use of a *k*-epsilon model for the turbulence. Assuming a turbulent intensity of 5 % in the pipe at the inlet, the kinetic energy and dissipation rate yielded $k = 0.375$ m²·s⁻², $\varepsilon = 3.59$ m²·s⁻² and a minimum wall distance of 0.0054 mm.

For the discharging process (solidification), in the hot exhaust gas domain, the inlet and outlet boundaries were assigned adiabatic walls, considering a virtual valve blocking the gas flow in the stovepipe once combustion is over. Though in reality the gas flow would not be fully blocked due to the need to evacuate the remaining exhaust gas from the charcoal burnout phase, this simplification minimized the heat losses through the inner pipe and eased the comparison between the different cases. As initial conditions, the hot gas domain was patched at 373 K, a relatively high temperature though still below the PCM's melting temperature. In the PCM domain, the fins and inner pipe were patched with a temperature of 395 K. Two different initial conditions were studied in the PCM domain: (1) starting from a constant and homogeneous temperature of 395 K above the PCM melting temperature and (2) starting from the liquid fraction and temperature fields as established after 6 hours of melting processes in the above-mentioned conditions, to mimic a dynamic case with sudden change of external conditions. In the first initial condition, the outer pipe temperature was set to 389 K, which is an average temperature obtained by the end of the above-mentioned melting processes.

Four fin lengths, attached to the inner pipe in the PCM domain, were studied under the described conditions. The four lengths corresponded to zero (no fins), 17.5 mm (one quarter of the PCM thickness), 52.5 mm (three quarters of the PCM thickness) and 70 mm (fin joining the inner pipe to the outer pipe). The 70-mm fins yielded the lowest packing factor with 97 % volume occupied by the PCM, considering 100 % with no fins. 35-mm fins (half of the PCM thickness) were investigated in a previous study (Soibam, 2017) and are not included here. The parametric study enabled us to understand the fin length's effects on melting and solidification and to determine the most relevant fin length for the given application with wood stoves.

2.7   Parameters for converged solutions

The temperature range for the phase change was set to 3 K, centered on 118 °C, since it enabled sufficient calculation stability, which narrower temperature ranges did not. It should be reminded that this temperature range is to some extent dependent on the mushy zone constant, as shown by Kheirabadi & Groulx (2015).

In the solution method, the PRESTO scheme was used for the pressure correction equation and the Semi-Implicit Pressure-Linked Equation (SIMPLE) algorithm for the pressure-velocity coupling. Momentum, turbulent kinetic and energy equations were computed using the first-order scheme. To enable converged solutions, the relaxation factors were set to 0.1 for liquid fraction, 0.3 for pressure and momentum, 0.8 for density, turbulent kinetic energy and turbulent dissipation rate, 0.9 for energy and 1 for body forces.

A sensitivity analysis on the choice of time step revealed that 1 s was a sufficiently small time step to simulate the behavior of the PCM during the melting process. However, a time step of 0.5 s for the solidification process provided better results for the solidification case.

3   Results and discussion

3.1   Liquid fraction

Figure 2 shows the effect of the fin length on the liquid fraction for 6 h of charge (melting) followed by a discharge (solidification). A 6-hour duration corresponds to a realistic average combustion duration of several batches using wood stoves. After that duration, the boundary conditions were changed in the inner pipe to trigger the discharge. Simulations running charging only (melting) revealed that with the 70-mm fins, 11.5 hours were needed to fully melt the PCM, and none of the other tested fin configurations reached full melting. In Figure 2, the liquid fraction with the 70-mm fins lies below the other configurations with fins until 6 hours into the charging process. The configuration with no fins, however, barely reached a liquid fraction of 0.6.
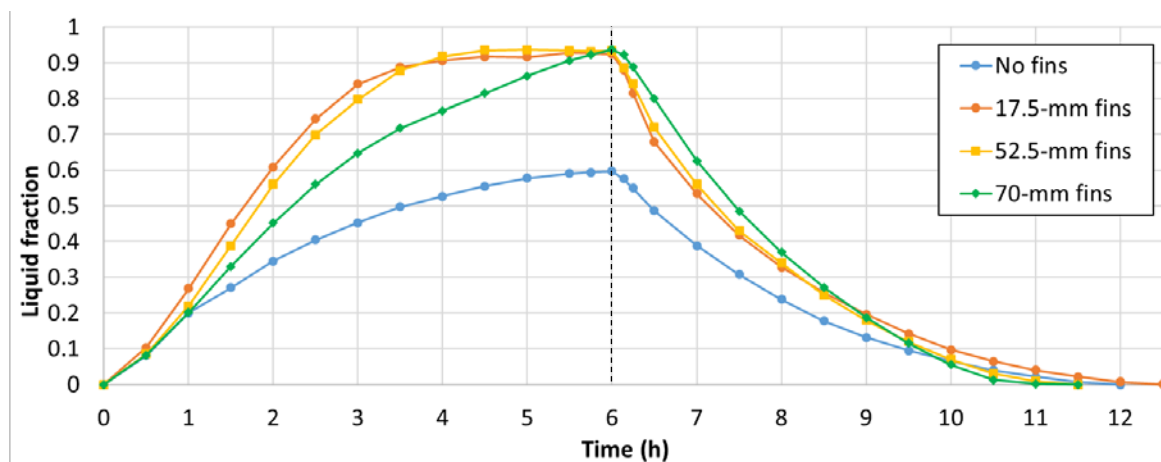
Figure 2: Effect of fin length on liquid fraction for 6 h of charge (melting) followed by a discharge (solidification).

The cases with 17.5-mm fins and 52.5-mm fins showed similar trends for the liquid fraction, with 17.5-mm fins slightly ahead for the first four hours. However, as the heat transfer from the hot exhaust gas continued, the liquid fraction for the 17.5-mm fins first stagnated and then slightly decreased instead of following the expected increasing trend. The same effect was observed for the case with 52.5-mm fins after five hours. This effect is due to the free convection effects, transporting the hot melted PCM through buoyancy to the top while the cooler melted PCM was transported to the bottom, eventually creating a sufficient vertical temperature gradient cooling down the lower part of the PCM block, below the melting temperature. This effect is amplified by the continuous exchange of heat between the melted PCM and the outer pipe which releases heat by radiation and convection to the room at an ambient temperature of 25 °C. This local re-solidification phenomenon in the lower part of the PCM domain was clearly observed in the 2D animated visualization of the liquid fraction of the charging phase.

During the discharging process, the configuration with 70-mm fins yields a significantly higher rate of solidification than all the other cases. With 70-mm fins, the PCM was fully solidified after 5 h, followed by the case with the 52.5-mm fins in 5.5 h, no fins in 6 h and 17.5-mm fins in 6.5 h. The case without fins showed the lowest rates of solidification.

Figure 3 shows the liquid fraction in the 2D axisymmetric model after one hour of charge, for the four tested fin lengths. For all configurations with fins, the effects of buoyancy, yielding free convection, were visible through the melted PCM accumulating under the fins. After one hour of charging, the melted PCM reached a sufficient volume to pass beyond some of the fins for the case with 17.5-mm fins. Without fins, the effects of free convection led to a noticeably higher melted fraction in the upper part of the PCM domain, close to the inner pipe. In comparison, the melted fraction in cases with fins was more homogeneously distributed.

No fins   *17.5-mm fins*   *52.5-mm fins*   *70-mm fins*
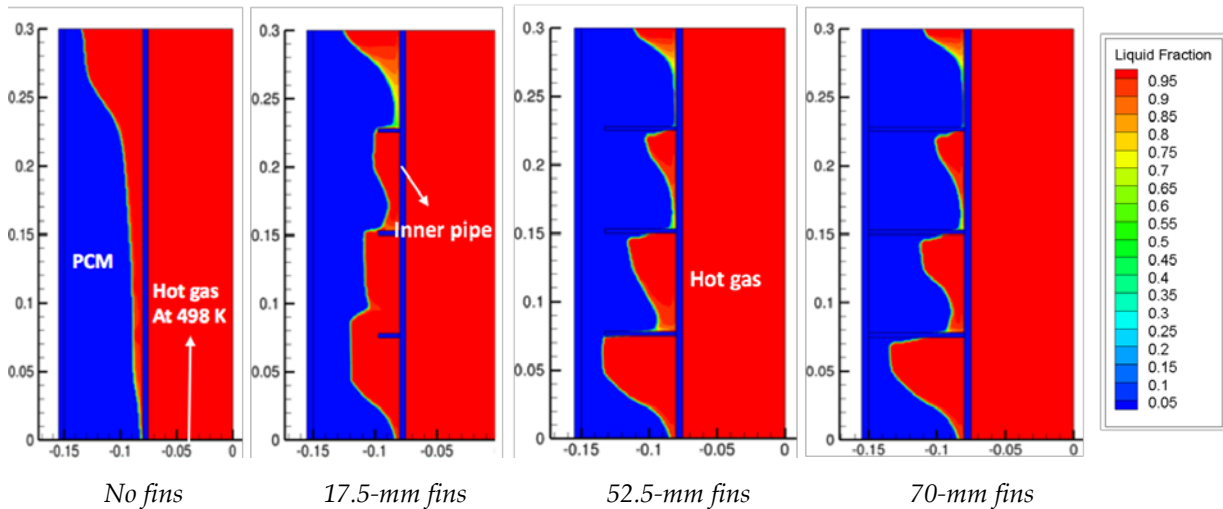
Figure 3: Effect of fin length on liquid fraction, one hour after start of melting process.

The boundary condition, set as constant velocity for the hot exhaust gas, may have led to an overestimated heat transfer to the lower part of the PCM domain. It could be improved, either by providing an established velocity profile, or modelling the gas inlet a few diameters upstream to establish the flow before reaching the PCM domain. A pressure-based inlet could be an alternative. However, due to the enhancement of heat transfer in the hot exhaust gas domain using longitudinal fins and the consequently higher effective thermal conductivity in the gas, the influence of the velocity field on the melting processes was not of high significance. Another aspect to consider is the location of the modelled heat exchanger, just above the hot stove, where higher heat transfer by conduction through the bottom of the inner pipe could be expected.

No fins   *17.5-mm fins*   *52.5-mm fins*   *70-mm fins*
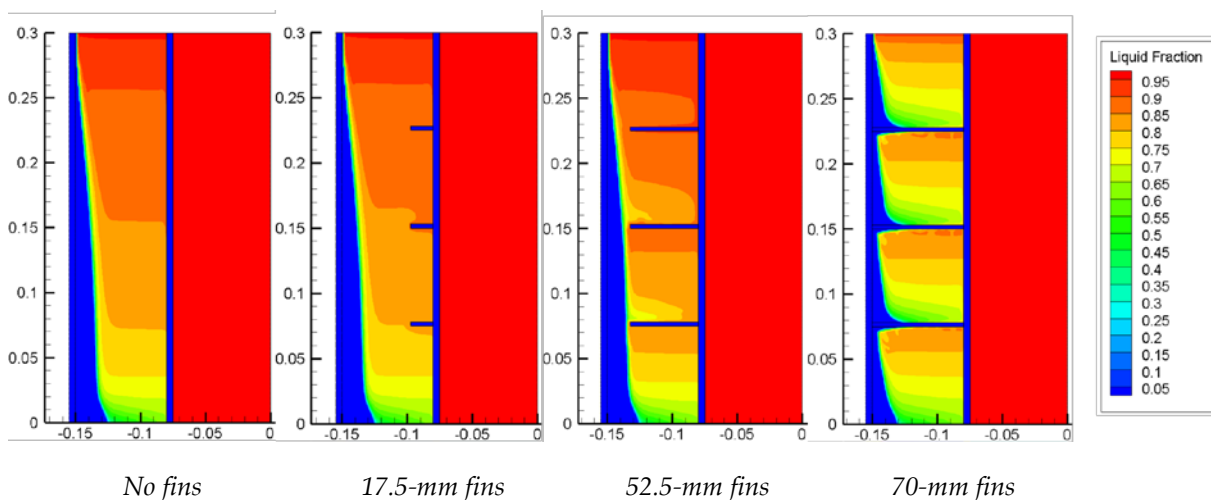
Figure 4: Effect of fin length on liquid fraction, 1 h after start of solidification (starting from fully liquid state).

Figure 4 shows the liquid fraction in the 2D axisymmetric model after one hour of discharge, for the four tested fin lengths. The solidification process progressed from the outer pipe wall since it was in contact with the surroundings maintained at 298 K. The solidification rate with 70-mm fins was significantly higher compared to the other cases. An important observation with regards to the solidification process is the significantly broader mushy zone compared to the melting process. The sharp mushy zone in the melting process was due to the convective heat transport playing a major role, while the solidification process is rather conduction-driven with almost no convective transport of melted PCM (Fleischer, 2015). This broadens the mushy zone where the PCM is in a slurry state, neither fully liquid nor solid.

3.2   Heat transfer to the surrounding

Figure 5 shows the effect of fin length on the average outer pipe wall temperature for 6 h of charge (melting) followed by a discharge (solidification). The temperature is dependent on the amount of heat absorbed or released by the PCM layer close to the outer pipe during the charging and discharging processes. The configuration with 70-mm fins allowed faster heating and higher maximum temperature compared to the other cases due to the direct contact between the inner pipe and the outer pipe yielding an enhanced heat transfer by conduction through the metallic fins. However, the outer pipe wall temperature never reached the PCM melting temperature within 6 hours, due to the incomplete melting of the PCM in all cases.
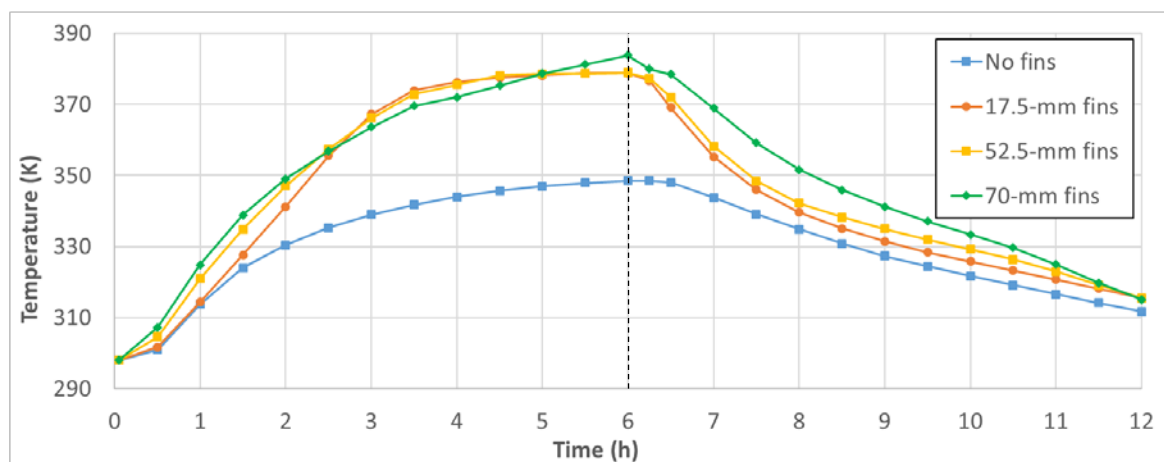
Figure 5: Effect of fin length on the average outer pipe wall temperature for 6 h of charge (melting) followed by a discharge (solidification).

The configurations with fins displayed different temperature profiles at first and thereafter reach the same wall temperature after ca. 2.5 hours of charging. The average outer wall temperature flattened with 17.5-mm fins and 52.5-mm fins after 4.5 hours, showing a close to overall thermal equilibrium in the system. During the discharge, the configuration with 70-mm fins dominated the other cases with respect to temperature, as well as decrease rate.

Figure 6 shows the effect of fin length on the heat transferred from the outer pipe to the room for 6 h of charge (melting) followed by a discharge (solidification). The convective and conductive heat transport in the cases with 17.5-mm fins and 52.5-mm fins interestingly yielded a higher heat output to the room from 2.5 h up to 5 h of charge compared to the case with fins connecting the heat source all the way to the outer pipe (70-mm). For the configuration with 17.5-mm fins and 52.5-mm fins, a thermal balance was nearly reached after 4.5 hours, when the amount of transferred heat flattened.

For the case with 70-mm fins, the heat transferred from the outer pipe wall became significantly larger than the other cases after 5 hours. However, this includes also the heat transferred directly from the hot gas to the room through the highly conductive fins, bypassing the PCM. This is critical for our application since it results in an early heat loss to the room, before it is needed, while less heat reaches the PCM in the charging phase.
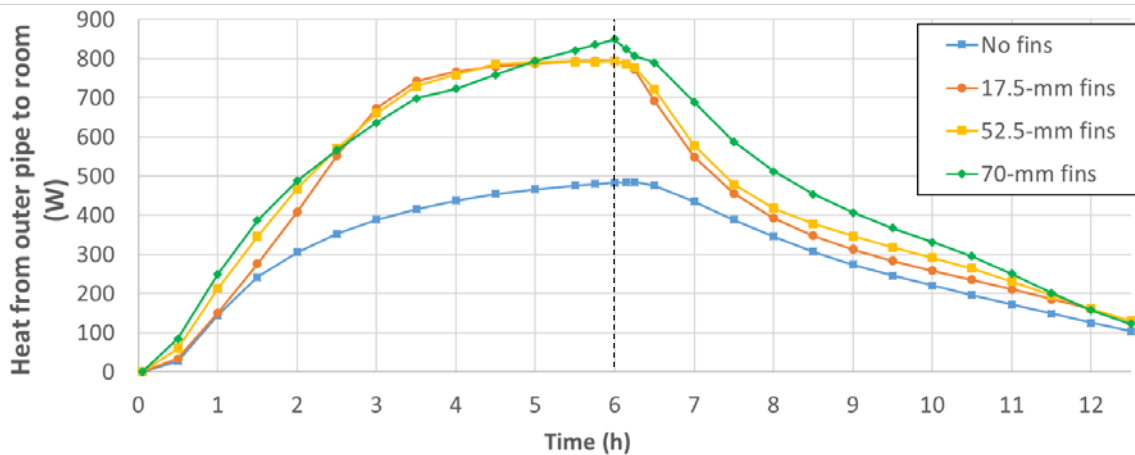
Figure 6: Effect of fin length on the heat transferred from the outer pipe to the room for 6 h of charge (melting) followed by a discharge (solidification).

The sudden change in supplied heat after 6 h marked the start of the discharging process. The heat loss to the inner pipe is minimal due to the blockage of the gas flow in the inner pipe. The 70-mm fins proved to yield the highest heat release to the room and the highest solidification rate. The change of gradient for this configuration during the first hour of discharge indicates the change between the heat transfer first shortly dominated by sensible heat and then by latent heat. The lowest solidification rate was associated with the configuration with no fins, though the total heat that can be released was naturally lower than for the other cases since a lower fraction of PCM was melted after 6 hours.

It should be noted that the heat transfer coefficient for convection of 25 $W \cdot m^{-2} \cdot K^{-1}$ for the outer pipe wall towards the room was probably over-estimated. A lower coefficient, closer to a regular free convection coefficient in the range of 5-10 $W \cdot m^{-2} \cdot K^{-1}$, may be more realistic and would yield a slower solidification rate by lowering the heat loss to the room. An even more realistic model would allow the convection coefficient to decrease with time, to include the transient influence of the significant convective hot air flow around the stove. Due to the generally large thermal inertia of the wood stoves, convection flows around them are typically large during the combustion phase and slowly decrease later as they cool down in the absence of combustion.

3.3   PCM temperature

Figure 7 shows the effect of fin length on the mass-weighted average PCM temperature for 6 h of charge (melting) followed by a discharge (solidification). All tested configurations with fins displayed a similar temperature profile for the first 4 hours of charging. Then, the configuration with 70-mm fins yielded the highest PCM temperature, potentially reaching local PCM overheating. With no fins, the average PCM temperature remained below the PCM melting temperature after 6 hours of charging. For the configurations with 17.5-mm and 52.5-mm fins, the average PCM temperature displayed a nearly flat temperature profile at 391 K after 3.5 h, which is the PCM phase change temperature. During this period, both

configurations displayed a slight decrease in average temperature. This corresponds to the local re-solidification phenomenon, as described in Section 3.1 and more visible in Figure 2.
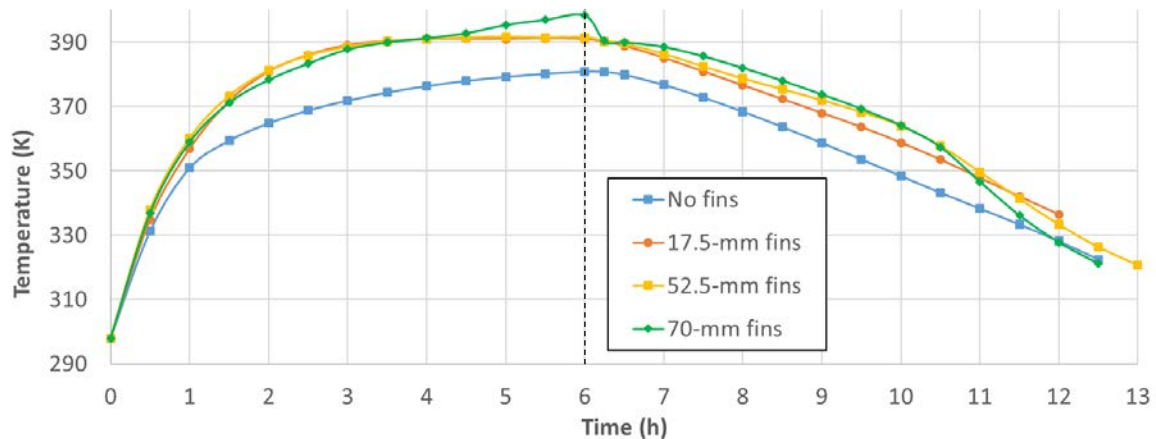
Figure 7: Effect of fin length on the mass-weighted average PCM temperature for 6 h of charge (melting) followed by a discharge (solidification).

During the discharge, after 6 hours of charge, the configuration with 70-mm fins displayed a sudden drop, followed by a slower drop in temperature getting larger and larger over time. The first sudden temperature drop was due to the loss of sensible heat followed by the slower drop due to the latent heat loss. The further increase in temperature drop was caused by the higher conductivity of the PCM as it solidified, enhancing the heat loss through the outer pipe. The latter explanation applies as well for the configurations with 52.5-mm fins. The effect was dramatically enhanced when the solidified PCM, solidifying from the outer wall inwards, came into contact with the fins, since it suddenly enhanced the heat transfer through the PCM. In comparison, the configuration with no fins showed a nearly linear temperature decrease.

3.4   Optimal configuration with regards to the application

The goal was to achieve a slow and close to complete melting of the PCM within a realistic combustion duration, for example 6 hours, while avoiding overheating the PCM beyond the degradation temperature. Then the discharge should allow a slow heat release of the stored latent heat within 6 to 10 hours. Among the four investigated fin lengths, the three configurations with fins clearly outperformed the case with no fins. The configurations with 17.5-mm and 52.5-mm fins provided a good trade-off for our application by charging the system within only 4.5 hours and then keeping the overall PCM temperature under critical conditions. Though the case with 70-mm fins yielded a significantly higher heat release to the room during the discharge, the early heat loss to the room during charging and the potential overheating of the PCM are a disadvantage.

Erythritol's degradation temperature is possibly too low for a batch combustion application displaying a high frequency of temperature variations and potentially higher maximum temperatures in the hot exhaust gas than tested here. Supercooling of erythritol was also reported in the literature (Höhlein et al., 2017) and was not implemented in the simulations. Though the problem might be minor in view of the large differences of temperature experienced by the system, experimental validation tests would be necessary. Another PCM may be considered in further studies.

Further investigation could also be conducted regarding the position of the radial fins. Reducing the interspace in the upward direction would, for example, enhance the heat transfer

from the inner pipe as the hot exhaust gas temperature decreases. The shape of the fins could also be more advanced to ensure an optimal heat transfer to the PCM. However, for the relatively low amount of heat to be stored without negatively interacting with the chimney draught, a functional solution should remain affordable.

4   Conclusions

A passive LHS system designed as a coaxial cylinder acting as a stovepipe located at the top of a wood stove was simulated by transient 2D axisymmetric CFD modelling with ANSYS FLUENT. The heat exchanger was equipped with internal radial metallic fins to enhance the conductivity and even-out the temperature distribution inside the PCM. Various fin configurations were evaluated through numerical simulations.

Regarding fin number and separation in the PCM domain, configurations with three equidistant radial fins along the 300-mm long inner pipe provided an effective heat distribution in the PCM. The effect of fin lengths was investigated through a parametric study using four different fin lengths within the PCM domain. Using 17.5-mm or 52.5-mm fins in the 70-mm PCM layer yielded the most effective results. The configuration enabled achieving a slow but close to complete melting of the PCM within a realistic combustion duration, while avoiding overheating the PCM beyond the degradation temperature. Then the discharge allowed a slow heat release of the stored latent heat for 6 to 10 hours.

A few recommendations were pointed out along the discussion of the results, notably the need to study more advanced fin configurations. Another remaining challenge is the potential thermal degradation of erythritol, occurring only 42 °C, or less, above the PCM melting temperature. This critical temperature may be reached in the layer close to the hot exhaust gas due to the highly transient combustion behavior of the batch-combustion stoves, endangering the durability of a practical LHS system.

Lastly, the mushy zone constant plays a major role on the modelling of melting processes due to its influence on the local convection effects enhancing the melting of the PCM. A finer tuning of this constant against experimental data would allow more realistic results.

5   Acknowledgements

References

Al-Abidi, A. A., Mat, S., Sopian, K., Sulaiman, M. Y., & Mohammad, A. T. (2013a). Internal and external fin heat transfer enhancement technique for latent heat thermal energy storage in triplex tube heat exchangers. *Applied Thermal Engineering, 53*(1), 147-156.

Al-Abidi, A. A., Mat, S., Sopian, K., Sulaiman, M. Y., & Mohammad, A. T. (2013b). Numerical study of PCM solidification in a triplex tube heat exchanger with internal and external fins. *International Journal of Heat and Mass Transfer, 61,* 684-695.

Almsater, S., Alemu, A., Saman, W., & Bruno, F. (2017). Development and experimental validation of a CFD model for PCM in a vertical triplex tube heat exchanger. *Applied Thermal Engineering,* 116, 344-354.

ANSYS. (2015). *Fluent Theory Guide, Release 16.1.*

Benesch, C., Blank, M., Scharler, R., Kössl, M., & Obernberger, I. (2015). *Transient CFD Simulation of Wood Log Stoves with Heat Storage Devices.* 21st European Biomass Conference and Exhibition.

Brent, A. D., Voller, V. R., & Reid, K. J. (1988). Enthalpy-porosity technique for modeling convection-diffusion phase change: Application to the melting of a pure metal. *Numerical Heat Transfer,* 13(3), 297-318.

Comini, G., Del Guidice, S., Lewis, R. W., & Zienkiewicz, O. C. (1974). Finite element solution of non-linear heat conduction problems with special reference to phase change. *International Journal for Numerical Methods in Engineering,* 8(3), 613-624.

Fleischer, A. S. (2015). *Thermal energy storage using phase change materials: fundamentals and applications*: Springer.

Georges, L., Skreiberg, Ø., & Novakovic, V. (2013). On the proper integration of wood stoves in passive houses: Investigation using detailed dynamic simulations. *Energy and Buildings,* 59(Supplement C), 203-213.

Gil, A., Medrano, M., Martorell, I., Lázaro, A., Dolado, P., Zalba, B., & Cabeza, L. F. (2010). State of the art on high temperature thermal energy storage for power generation. Part 1—Concepts, materials and modellization. *Renewable and Sustainable Energy Reviews,* 14(1), 31-55.

Hoshi, A., Mills, D. R., Bittar, A., & Saitoh, T. S. (2005). Screening of high melting point phase change materials in solar thermal concentrating technology based on CLFR. *Solar Energy,* 79(3), 332-339.

Höhlein, S., König-Haagen, A., & Brüggemann, D. (2017). Thermophysical Characterization of MgCl(2)·6H(2)O, Xylitol and Erythritol as Phase Change Materials (PCM) for Latent Heat Thermal Energy Storage (LHTES). *Materials,* 10(4), 444.

Kaizawa, A., Maruoka, N., Kawai, A., Kamano, H., Jozuka, T., Senda, T., & Akiyama, T. (2008). Thermophysical and heat transfer properties of phase change material candidate for waste heat transportation system. *Heat and Mass Transfer,* 44(7), 763-769.

Kheirabadi , A. C., & Groulx, D. (2015). Simulating phase change heat trasnfer using Comsol and Fluent: Effect of the mushy-zone constant. 7(5-6), 427-440.

Kristjansson, K., Næss, E., & Skreiberg, Ø. (2016). Dampening of wood batch combustion heat release using a phase change material heat storage: Material selection and heat storage property optimization. *Energy,* 115, Part 1, 378-385.

Mandl, C., & Obernberger, I. (2017). *Guidelines for heat storage units based on Phase Change Materials (PCM).*

Mehling, H., & Cabeza, L. F. (2008). *Heat and cold storage with PCM.* Springer, Berlin, Heidelberg.

Sharma, A., Tyagi, V. V., Chen, C. R., & Buddhi, D. (2009). Review on thermal energy storage with phase change materials and applications. *Renewable and Sustainable Energy Reviews,* 13(2), 318-345.

Soibam, J. (2017). *Numerical Investigaton of a Phase Change Material Heat Exchanger for Small-Scale Combustion Appliances.* (Master Degree), NTNU, Trondheim, Norway.

Voller, V. R. (1990). Fast implicit finite-difference method for the analysis of phase change problems. *Numerical Heat Transfer, Part B: Fundamentals,* 17(2), 155-169.

Zielke, U., Bjerrum, M., & Nørgaard, T. (2013). *Slow Heat Release - Brændeovn med salthydratvarmelager - Miljøprojekt nr. 1438.*

Özişik, N. (1994). *Finite Difference Methods in Heat Transfer.* Taylor & Francis.